CrossMark

ORIGINAL PAPER

Electrical and Dielectrical Properties of Low-Temperature-Synthesized Nanocrystalline Mg^{2+}-Substituted Cobalt Spinel Ferrite

Vithal Vinayak[1] · Pankaj P. Khirade[2] · Shankar D. Birajdar[2] · R. C. Alange[3] ·
K. M. Jadhav[2]

Abstract Nanocrystalline samples of $Co_{1-x}Mg_xFe_2O_4$ ($x = 0.0$, 0.25, 0.50, 0.75, and 1.0) ferrite were synthesized by wet chemical sol-gel auto combustion method. The spinel cubic phase formation of $Co_{1-x}Mg_xFe_2O_4$ ferrite samples was confirmed by X-ray diffraction (XRD) data analysis. All the Bragg planes observed in XRD pattern belong to the cubic spinel structure of ferrite. The microstructural studies were investigated through scanning electron microscopy (SEM) technique. Pellets of Co–Mg ferrite were used to study the electrical and dielectric properties. The DC electrical resistivity studies of the prepared $Co_{1-x}Mg_xFe_2O_4$ ($x = 0.0$–1.0) ferrite samples were carried out in the temperature range of 300–873 K using a standard two-probe method. Ferrimagnetic to paramagnetic transition temperature known as Curie temperature (T_c) for all samples was noted from resistivity data. The Curie temperature decreases linearly as concentration of magnesium content is increased. The activation energy below and above T_c was calculated. The dielectric parameters such as dielectric constant (ε'), dielectric loss (ε''), and loss tangent (tan δ) were measured with frequency at room temperature in the frequency range 10 kHz to 1 MHz. The dielectric constant (ε') measurements with increasing frequency show two peaks at room temperature of measurements for all samples under investigation. The peaks observed show compositional dependences as a function of frequency. The observed behavior in the electrical and dielectric behavior of nanocrystalline $Co_{1-x}Mg_xFe_2O_4$ spinel ferrites is discussed in this work.

1 Introduction

Recently, nanocrystalline materials are focused by scientists and technologists because of their prospective and wide range of applications. Ferrites have good electrical and dielectric properties. The electrical transport properties of ferrites provide information suitable for the specific applications of ferrite in electrical and electronic devices. The ferrimagnetic cubic spinel ferrites are excellent magnetic and dielectric materials. The ferrite materials substituted with different cations have become the most important because of their both fundamental and technological applications such as telecommunications, power transformers, EMI suppressors, SPMS, microwave devices, and read/write heads [1, 2]. The dielectric properties of ferrites can be tailored either by changing the microstructure or by different synthesis techniques. The spinel ferrites exhibit interesting electrical and dielectric properties in the nanocrystalline form compared to those of bulk form. It is a well-known fact that the electrical properties of spinel ferrites strongly depend on temperature while that of dielectric properties on frequency.

Polycrystalline ferrites are very high-quality dielectric materials and having various technological applications that

✉ K. M. Jadhav
drjadhavkm@gmail.com

1 Department of Chemistry, B. S .S. Arts & Science College, Makni, Tq: Lohara, Osmanabad, (M.S.), India

2 Department of Physics, Dr. Babasaheb Ambedkar Marathwada University, Aurangabad, (M.S.), India

3 Department of Physics, Shri. Madhavrao Patil Mahavidyalaya, Murum, Omerga, Osmanabad (M.S.), India
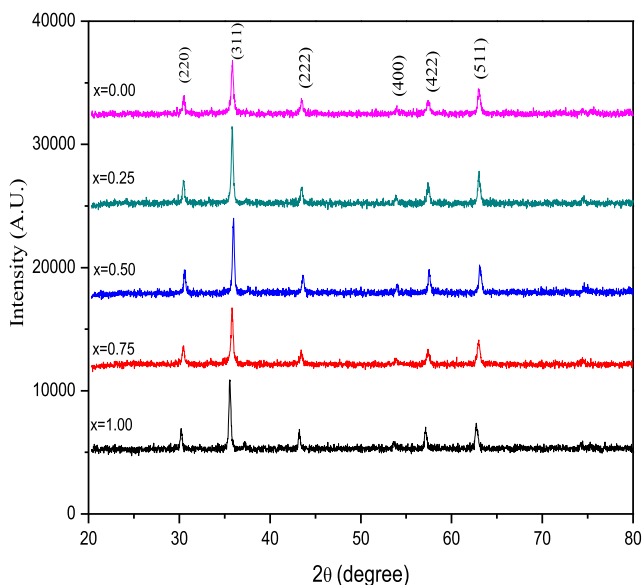
Fig. 1 X-ray diffraction patterns of $Co_{1-x}Mg_xFe_2O_4$ ($x = 0.0 - 1.0$) system (recorded at room temperature)

ranges from microwave to radio frequencies [3–6]. The quality of ferrite powder has a strong influence on the performance of the device. Thus, the study of electrical conduction and dielectric properties at different frequencies, temperatures, and compositions will give valuable information about the kind and amount of additives required to obtain high-quality ferrite materials.

Electrical switching in polycrystalline ferrites was reported by Yamashiro [7]; also, similar reports are presented by Murthy [8] for Mg–Cu–Zn ferrite. The dielectric behavior of Cu–Zn, Li–Zn, and Mg–Zn ferrite systems as a function of frequency was reported by many workers [9–12]. The electrical properties of Mg–Mn ferrites can be possibly upgraded by incorporating suitable cations. Mg–Mn ferrites are considered as the most versatile ferrites due to their high resistivity and low eddy current losses for high-frequency applications [13]. As the properties of ferrites are known to be sensitive to their composition and the processing technique used to synthesize them, many workers have studied mixed ferrites by standard ceramic technique [14, 15], chemical co-precipitation method [16], sol-gel method [17], and ball-milling method [18]. Although, there are

reports on the electrical and dielectric behavior of mixed spinel ferrite but rare work has been reported on Co–Mg mixed spinel ferrite.

The electrical conductivity of spinel ferrite is of prime importance as it provides valuable information about the conduction mechanism. Studies of dielectric parameters of cubic spinel ferrites are important in understanding electrical conduction and polarization phenomenon. Therefore, in the present work, a systematic study of the electrical conductivity of mixed Co–Mg spinel ferrite system from room temperature to beyond Curie temperature and dielectric properties as function of frequency was undertaken.

2 Experimental

2.1 Synthesis

A nominal composition of $Co_{1-x}Mg_xFe_2O_4$ with x varying from 0.0 to 1.0 in steps of 0.25 has been prepared by sol-gel auto combustion method. Analytical-grade (AR) chemicals such as cobalt nitrate ($Co(NO_3)_2 \cdot 6H_2O$), magnesium nitrate ($Mg(NO_3)_2 \cdot 6H_2O$), ferric nitrate ($Fe(NO_3)_3 \cdot 9H_2O$), and citric acid ($C_6H_8O_7$) were used for the synthesis. Citric acid ($C_6H_8O_7$) was used as a fuel. The metal nitrates-to-fuel (citric acid) ratio was taken as 1:3. Ammonia solution was added to maintain the pH 7. The temperature required for the synthesis of Co–Mg ferrite nanoparticles was low that is around 110 °C. The as-synthesized powder is sintered at 550 °C for 4 h and then used for further investigations.

2.2 Characterizations

The prepared samples were characterized by X-ray diffraction (XRD—Rigaku) at room temperature. The XRD patterns were recorded at room temperature in the 2θ range of 20° to 80° using Cu-Kα radiation ($\lambda = 1.54056$ Å). Morphology of the prepared samples was studied using a scanning electron microscope (SEM) JEOL-JSM 840 model at an operating voltage 20 kV. An electrical conductivity mechanism in prepared ferrites was analyzed by studying their DC electrical resistivity. The simple and easy technique to study electrical property of the pelletized (10-mm diameter and 3-mm thickness) ferrite samples is

Table 1 Lattice constant (a), X-ray density (d_x), bulk density (d_B), porosity ($P\%$), unit cell volume (V), and average particle size (t) of $Co_{1-x}Mg_xFe_2O_4$ system (where $x = 0.0$–1.0)

Composition x	a(Å)	d_x(gm/cm^3)	d_B (gm/cm^3)	$P\%$	V(Å^3)	t
0.00	8.389	5.279	3.10	16.59	590.38	32.43
0.25	8.381	5.236	3.20	18.30	588.67	31.81
0. 50	8.373	4.916	3.27	23.88	587.11	24.13
0.75	8.367	4.731	3.32	25.22	585.77	17.78
1.00	8.360	4.546	3.36	26.69	584.30	10.67

two-probe technique. Pellets of samples were used for measuring the DC electrical resistivity. Pellets were polished for smooth parallel faces and coated with silver paste to ensure good ohmic contact. Using the two-probe method, the resistivity for all samples was calculated. The various parameters such as activation energy and Curie temperature have been studied. The dielectric properties of all the samples were measured using the LCR-Q meter (HIOKI 3532-50, Japan) as a function of frequencies. The dielectric constant, dielectric loss, and dielectric loss tangent were obtained.

3 Results and Discussion

3.1 Structural Studies

Structural studies of $Co_{1-x}Mg_xFe_2O_4$ (with $x = 0.0, 0.25, 0.50, 0.75$, and 1.0) ferrite nanoparticles under investigation were carried out using X-ray diffraction technique. All the samples exhibit single-phase cubic spinel structure without any impurity phases. Figure 1 depicts the X-ray diffraction patterns of the present samples. The pattern confirms the formation of single-phase cubic spinel structure as the corresponding planes such as (220), (311), (222), (400), (422), (511), and (440) are present in it. Various crystalline parameters like interplanar spacing (d), X-ray density (d_x), lattice constant (a), unit cell volume (V), and average crystalline sizes (t) have been calculated from XRD data.

The average particle size (t) was calculated by using Debye-Scherrer's formula using XRD data and is obtained to be in the range of 10–32 nm. Table 1 gives various structural parameters such as lattice constant (a), X-ray density (d_x), bulk density (d_B), porosity ($P\%$), unit cell volume
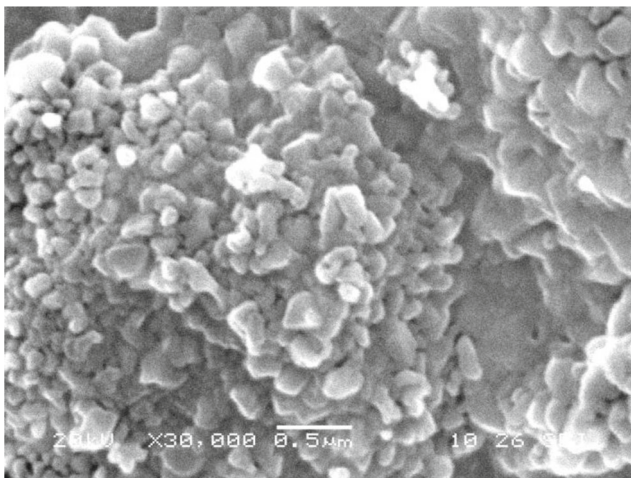
Fig. 2 Typical SEM image of $Co_{0.50}Mg_{0.50}Fe_2O_4$

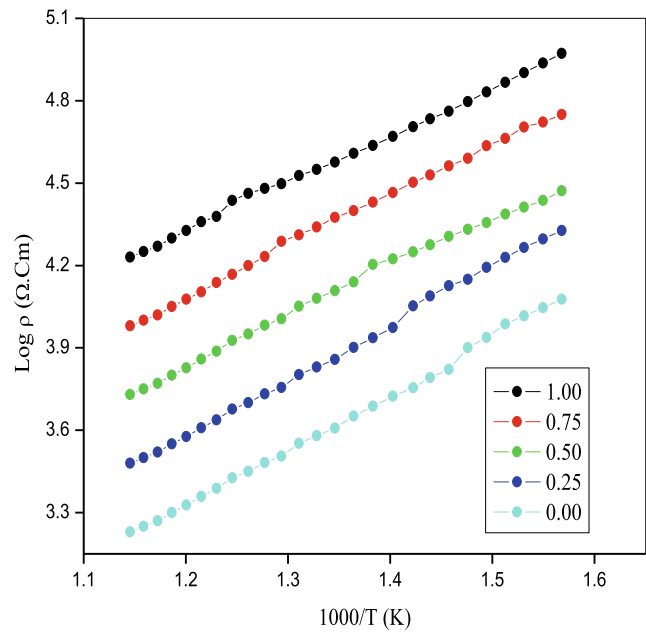**Fig. 3** Variation of DC electrical resistivity with reciprocal of temperature for $Co_{1-x}Mg_xFe_2O_4(x = 0.0 - 1.0)$ system

(V), and average particle size (t) of $Co_{1-x}Mg_xFe_2O_4$ system. The lattice constant (a) is calculated by using $a = d\left(h^2 + k^2 + l^2\right)^{1/2}$; from Table 1, it is clear that the lattice constant (a) decreases with magnesium substitution as expected. The decreasing behavior of lattice constant with Mg^{2+} content is because of the replacement of Mg^{2+} ions having comparatively smaller ionic radius (0.72 Å) than that of Co^{2+} (0.74 Å). The variation of the lattice parameter (a) as a function of Mg^{2+} ion concentration (x) in the $Co_{1-x}Mg_xFe_2O_4$ matrix follows Vegard's law [19]. The X-ray density (d_x) was calculated from lattice parameter (a), molecular weight, and Avogadro's number [20]. X-ray density of pure cobalt ferrite (Table 1) was found to be 5.279 g/cm³ which is in reported range. The value of d_x decreases with increase in magnesium substitution. Bulk density (d_B) of the investigated sample was measured using the Archimedes principle [21], and its lower value than X-ray density is attributed to the pore formation during synthesis processes [22]. It can be understood from Table 1 that the bulk density increases with increase in magnesium substitution. Porosity ($P\%$) of magnesium-substituted cobalt ferrite was estimated from the values of d_x and d_B using relation [23]. The increase in ($P\%$) with increase in magnesium substitution is attributed to decrease in X-ray density and the porosity values lie in between 16 and 26 %.

Figure 2 shows typical morphological pattern of the prepared magnesium-substituted cobalt spinel ferrite nanoparticles taken by SEM for the sample $x = 0.50$. Evidently,

Table 2 Activation energy in paramagnetic (E_p) and ferrimagnetic (E_f) region and activation energy (ΔE) and Curie temperature (T_c) for $Co_{1-x}Mg_xFe_2O_4$ system

Composition x	ρ (kΩ) at 873 K	E_p (eV)	E_f (eV)	ΔE (eV)	T_c (K)
0.00	0.1699	0.9055	0.5838	0.3217	803
0.25	0.3022	0.5246	0.2374	0.2878	773
0.50	0.5374	0.7254	0.5075	0.2179	723
0.75	0.9556	0.7320	0.5453	0.1897	703
1.00	1.6994	0.6370	0.4810	0.1560	673

from the SEM image of the sintered magnesium-substituted cobalt spinel ferrite samples, it was seen that the morphology of the particles were almost spherical in shape, but agglomerated to some extent due to the interaction between magnetic nanoparticles. It can be observed that grains of uniform size are distributed throughout the surface which exhibits decreasing trend together with magnesium substitution. The formation of nanosized crystallites was confirmed through SEM images. The average grain size calculated from linear intercept method was found to be in the nanometer range of 45–66 nm.

3.2 DC Electrical Resistivity

The DC electrical resistivity studies of the prepared $Co_{1-x}Mg_xFe_2O_4$ ($x = 0.0$, 0.25, 0.50, 0.75, and 1.0) ferrite samples were carried out in the temperature range of 300–873 K. The resistivity for each sample at the same temperature was calculated, and logarithm of the resistivity (log ρ) was plotted as a function of reciprocal of temperature (1000/T). Figure 3 shows the variation of logarithm of resistivity as a function of reciprocal of temperature. It is evident from Fig. 3 that the resistivity decreases with increasing temperature obeying Arrhenius relation [24]. This confirms the semiconducting behavior of magnesium-substituted cobalt spinel ferrite samples under investigation. DC electrical resistivity of the samples was found to be increased with the increase in magnesium content x as mentioned in Table 2.

3.2.1 Activation Energy

The slope of the linear plots drawn of log (ρ) vs 1000/T gives the activation energy of the samples. The activation energy was calculated for each sample and the values are tabulated in Table 2 along with the other parameters. Activation energy is found to decrease from 0.3217 to 0.1560 eV with increases in magnesium substitution from $x = 0.0$, 0.25, 0.50, 0.75, and 1.0. The decrease in activation energy may be due to the creation of smaller number of oxygen vacancies; Fig. 2 shows the variation of activation energy with magnesium content x.

3.2.2 Curie Temperature

The graphs drawn in Fig. 3 show slope at particular temperature indicating that sample undergoes change from ferrimagnetism to paramagnetism. The temperature at which changes its state may correspond to Curie temperature. The Curie temperature of each sample is mentioned in Table 2. From the table, it is clear that Curie temperature decreases from 803 to 673 K with magnesium substitution x. The similar behavior of the present samples is analogous to that of reported in the literature [25, 26].

3.3 Dielectrical Studies

Dielectric properties of $Co_{1-x}Mg_xFe_2O_4$ ($x = 0.0$, 0.25, 0.50, 0.75, and 1.0) ferrite nanopowders synthesized by sol-gel auto combustion technique and sintered at 550 °C were studied at room temperature multifrequency LCR-Q meter. The capacitance (C) and loss tangent (tan δ) were measured in the frequency range 10 kHz to 1 MHz. Figures 4, 5 and 6 respectively shows the variation of dielectric constant (ε'), dielectric loss (ε''), and loss tangent (tan δ) with frequency at room temperature in the frequency range 10 kHz to 1 MHz.
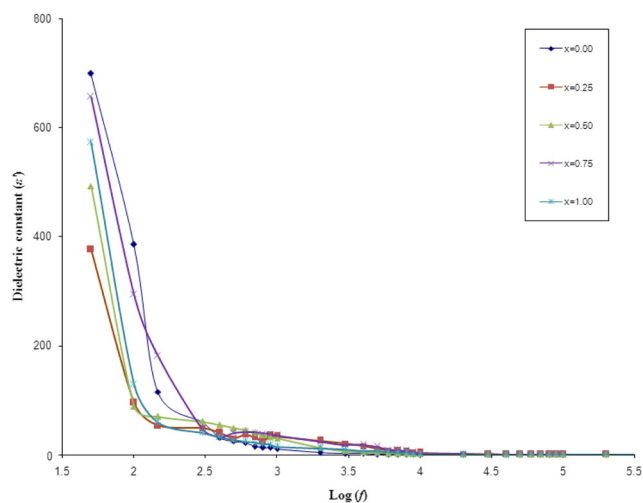
Fig. 4 Variation of dielectric constant (ε') with frequency at room temperature of $Co_{1-x}Mg_xFe_2O_4(x = 0.0 - 1.0)$
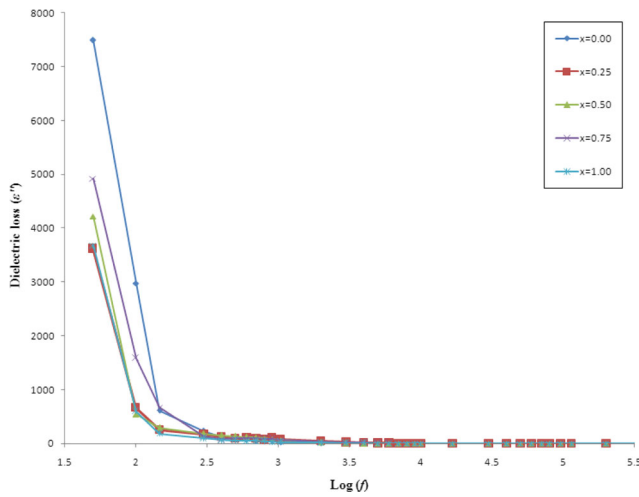
Fig. 5 Variation of dielectric loss (ε'') with frequency at room temperature of $Co_{1-x}Mg_xFe_2O_4 (x = 0.0 - 1.0)$

3.3.1 Dielectric Constant (ε')

The dielectric constant (ε') was calculated using the following formula:

$$\varepsilon' = \frac{Ct}{\varepsilon_0 A} \tag{1}$$

where, C is the capacitance of pellet, t is the thickness of the specimen, A is the area of cross section of the pellet, and ε_0 is the permittivity of the free space.

The dependence of dielectric constant with frequency is shown in Fig. 4. It is observed that the dielectric constant is high in the range of low frequency and it decreases with frequency. The reasons of high value of dielectric constant at low frequencies may be due to dislocations, voids, and defects present in the crystal structure of nanoferrites. The decrease in dielectric constant with increasing frequency is due to the fact that at higher frequencies, any effect contributing to polarization is found to show lagging behind the applied field. When frequency is increased beyond a certain frequency limit, the electron hopping cannot follow the electric field fluctuations and causes decrease in the dielectric constant. At high frequencies, the value of dielectric constant is low because it comes from the grains having a small value of dielectric constant due to low resistivity and becomes less dependent on frequency. The observed variation of dielectric constant with frequency can be attributed to the space charge polarization, which is due to an inhomogeneous dielectric structure as discussed by Maxwell and Wagner and is in agreement with Koops' [27] phenomenological theory.

Increase in magnesium substitution content x causes dielectric constant to decrease, in the low frequency range. At room temperature, the dominant mode of conduction is electron hopping between Fe^{2+} and Fe^{3+} and the number of Fe^{2+} ions decreases with increasing x. With decreasing ferrous ions which are responsible for polarization, a decrease in dielectric constant is expected with x. Analogous results are observed previously for similar materials.

3.3.2 Dielectric Loss (ε'')

The dielectric loss (ε'') is also measured in terms of tangent loss factor ($\tan\delta$) and ε' defined by the following relation,

$$\varepsilon'' = \varepsilon' \tan\delta \tag{2}$$

The dependence of dielectric loss with frequency is shown in Fig. 5. It is observed from Fig. 5 that dielectric loss decreases exponentially with increase in frequency. At low frequency, the dielectric loss shown much higher values compared to the values at high-frequency region. The decrease in dielectric loss is similar to the decrease in dielectric constant. The observed behavior of dielectric loss is similar to that reported in the literature. It is reported in literature that the values of dielectric loss depend on a number of factors such as Fe^{2+} contents, structural homogeneity, and stoichiometry, which in turn depend on the synthesis methods and composition.

3.3.3 Dielectric Loss Tangent ($\tan\delta$)

Figure 6 depicts the variation of dielectric loss tangent as a function of frequency. It is observed from Fig. 6 that like dielectric constant, dielectric loss tangent also decreases exponentially with increase in frequency. The decrease of dielectric loss tangent with increase in frequency is due to
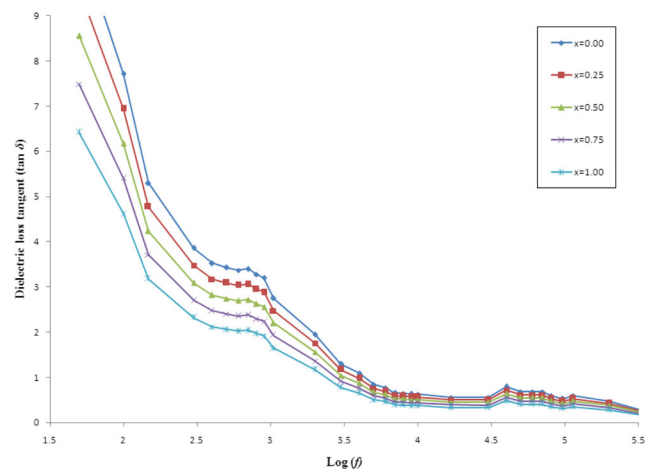

Fig. 6 Variation of dielectric loss tangent ($\tan\delta$) with frequency at room temperature of $Co_{1-x}Mg_xFe_2O_4 (x = 0.0 - 1.0)$

the fact that there is a strong association between dielectric behavior of ferrites and the conduction mechanism. Plots of dielectric loss tangent (tan δ) versus logarithm of frequency (log f) do not show any peak with frequency in the frequency range under study, for any of the samples. The absence of the peak is perhaps due to small contribution of dielectric permittivity to show any observable variation of loss factor with frequency. Further, the decrease of tan δ with increasing frequency is attributed to the fact that the hopping frequency of charge carriers cannot follow the changes of the externally applied electric field beyond a certain frequency limit.

The obtained results are in good agreement with the literature reports [27]. Similar dielectric properties were observed for the Zn–Mg–Cu and Mg–Zn–Co spinel ferrites [28, 29].

4 Conclusions

Co$_{1-x}$Mg$_x$Fe$_2$O$_4$ (x = 0.0, 0.25, 0.50, 0.75, and 1.0) nanocrystalline ferrite samples were synthesized using sol-gel auto combustion technique and found to have a single-phase cubic spinel structure. The lattice constant has been observed to decrease linearly with magnesium substitution obeying Vegard's law. The values of lattice constant and X-ray density with increase in Mg^{2+} concentration is in reported range. The bulk density is quite low as compared to X-ray density. The grain size determined by linear intercept method from scanning electron microscopy technique is of the order of nanometer range. DC electrical resistivity decreases with increase in temperature obeying Arrhenius relation. The DC electrical resistivity measurements show that the resistivity increases with substitution of magnesium in cobalt ferrite increases. The dielectric behavior shows strong frequency as well as composition dependence. The dielectric constant, dielectric loss, and dielectric loss tangent all decrease exponentially with increase in frequency. The decrease in loss tangent by increasing frequency may be ascribed to the Maxwell-Wagner polarization and conduction mechanism. At lower frequencies, it is observed that the dielectric properties are high.

References

1. Goldman, A.: Modern Ferrite Technology, pp. 375–386. Springer, US (2006)
2. Vijaya Kumar, K., Ravinder, D.: Mater. Lett. **52**, 166 (2002)
3. Yang, Z.H., Li, Z.W., Yang, Y.H., Liu, L., Kong, L.B.: J. Magn. Magn. Mater. **331**, 232–236 (2013)
4. Cao, X., Sun, K., Sun, C., Leng, L.: J. Magn. Magn. Mater. **321**, 2896–2901 (2009)
5. Iqbal, M.J., Ahmad, Z., Meydan, T., Melikhov, Y.: J. Magn. Magn. Mater. **324**, 3986–3990 (2012)
6. Kostishina, V.G., Vergazovb, R.M., Andreevb, V.G., Bibikovc, S.B., Morchenkoa, A.T., Kanevaa, I.I., Maiorova, V.R.: Russ. Microlectron. **41**(8), 469–473 (2012)
7. Yamashiro, T.: J. Appl. Phys. **12**, 148 (1973)
8. Murthy, S.R.: Bull. Mater. Sci. **24**(4), 379–383 (2001)
9. Josyulu, O.S., Sobhanadri, J.: Phys, Stat. Sol. (a) **59**, 323 (1980)
10. Ravinder, D., Murthy, S.R., Mulay, V.N., Reddy, K.B.: Phys. Status Solidi (a) **134**, 273 (1992)
11. El Hiti, M.A., Ahmed, M.A., Masud, M.M., Attia, S.M.: J. Magn. Magn. Mater. **150**, 399 (1995)
12. Ravinder, D., Latha, K.: Mater. Lett. **41**, 247 (1999)
13. Parvatheeswara Rao, B., Rao, K.H.: J. Mater. Sci. Lett. **22**, 1607–1608 (2003)
14. Singh, M., Sud, S.P.: Mater. Sci. Eng. B **83**, 180 (2001)
15. Kim, G.-Y., Jeon, J.-H., Kim, M.-H., Suvorov, D., Choi, S.-Y.: Met. Mater. Int. **19**(6), 1209–1213 (2013)
16. Ebrahimi, M., Shahraki, R.R., Seyyed Ebrahimi, S.A., Masoudpanah, S.M.: J. Supercond. Nov. Magn. **27**, 1587–1592 (2014)
17. Raut, A.V., Barkule, R.S., Shengule, D.R., Jadhav, K.M.: J. Magn. Magn. Mater. **358–359**, 87–92 (2014)
18. Zhenyu, L., Guangliang, X., Min, L., Ahniyaz, A., Yoshimura, M.: J. Wuhan Univ. Technol. Mater. Sci. Ed., 151–153 (2008)
19. Kumar, P., Mishra, P., Sahu, S.K.: vol. 2 (2011)
20. Aghav, P.S., Dhage, V.N., Mane, M.L., Shengule, D.R., Dorik, R.G., Jadhav, K.M.: Phys., B, Condens. Matter **409**, 4350 (2011)
21. Shinde, T.J., Gadkari, A.B., Vasambekar, P.M.: J. Mater. Sci. Mater. Electron. **21**, 120 (2010)
22. Haque, M.M., Huq, M., Hakim, M.A.: J. Indian Phys. **78 A**(3) (2004)
23. Lakhani, V.K., Pathak, T.K., Vasoya, N.H., Modi, K.B.: Solid State Sci. **13**, 539 (2011)
24. Yang, H., Zhang, X., Ao, W., Qiu, G.: Mater. Res. Bull. **39**(6), 833–883 (2004)
25. Kumar, G., Sharma, S., Kotnala, R.K., Shah, J., Shirsath, S.E., Batoo, K.M., Singh, M.: J. Mol. Struct. **1051**, 336–344 (2013)
26. Zaki, H.M., Al-Heniti, S., AlShehri, N.: Physica B **436**, 157–163 (2014)
27. Koops, C.G.: Phys., Rev. **83**, 1920 (1951)
28. Verma, K., Kumar, A., Varshney, D.: Curr. Appl. Phys. **13**, 467–473 (2013)
29. Hashim, M., Meena, S.S., Kotnala, R.K., Shirsath, S.E., Bhatt, P., Kumar, S., Şentürk, E., Kumar, R., Gupta, N., Alimuddin: J. Magn. Magn. Mater. **360**, 21–33 (2014)